Desalination and Water Treatment
www.deswater.com

doi: 10.5004/dwt.2019.23678

151 (2019) 56–65
May

Synthesis of Bi_2O_3/Bi_2WO_6 composites using single-step solvothermal method: determinations of surface characteristics and photocatalytic activity

Chung-Hsin Wu[a,*], Chao-Yin Kuo[b], Cheng-Di Dong[c], Chiu-Wen Chen[c], Yi-Li Lin[d], Chuan-Yu Liu[a]

[a]*Department of Chemical and Materials Engineering, National Kaohsiung University of Science and Technology, 415 Chien Kung Road, Kaohsiung, Taiwan, Tel. 886-7-3814526; Fax: 886-7-3830674; emails: wuch@nkust.edu.tw (C.-H. Wu), fiy2136sea@gmail.com (C.-Y. Liu)*
[b]*Department of Safety, Health and Environmental Engineering, National Yunlin University of Science and Technology, Yunlin, Taiwan, Tel: 886-5-5347311; email: kuocyr@ms35.hinet.net*
[c]*Department of Marine Environmental Engineering, National Kaohsiung University of Science and Technology, Kaohsiung, Taiwan, Tel. 886-7-3617141; emails: cddong@nkust.edu.tw (C.-D. Dong), cwchen@nkust.edu.tw (C.-W. Chen)*
[d]*Department of Safety, Health and Environmental Engineering, National Kaohsiung University of Science and Technology, Kaohsiung, Taiwan, Tel. 886-7-6011000; email: yililin@nkust.edu.tw*

Received 5 November 2018; Accepted 24 December 2018

ABSTRACT

Bi_2O_3, Bi_2WO_6 (BW) and Bi_2O_3/Bi_2WO_6 composites (BBWs) were synthesized by the single-step solvothermal method. Numerous Bi_2O_3/BW molar ratios were used to generate various BBWs and their surface characteristics and photocatalytic activities were measured and compared. Ethylene glycol was used as a solvent in the solvothermal process and C.I. Reactive Red 2 (RR2) was the target pollutant. The surface properties of BBWs were elucidated by X-ray diffraction, UV-vis spectrophotometry, scanning electron microscopy, transmission electron microscopy, energy dispersive X-ray spectroscopy, specific surface area analysis, zeta potential analysis and X-ray photoelectron spectroscopy. The effects of photocatalyst dosage, pH and RR2 concentration on RR2 photodegradation were also elucidated. The RR2 photodegradation rate in all BBWs systems under simulated solar light irradiation exhibited pseudo-first-order kinetics and a molar ratio of Bi_2O_3/BW of 0.5 (0.5 BB) yielded the highest photocatalytic activity, which was approximately 6.1 times higher than that of BW. The RR2 photodegradation efficiency increased with the photocatalyst dosage; it declined as the RR2 concentration or pH increased. The enhanced photocatalytic activity of BBWs was attributed to the effective separation of electron-hole pairs between Bi_2O_3 and BW; holes and superoxide radicals were the dominant active species in the photocatalytic system.

Keywords: Bi_2WO_6; Bi_2O_3; Solvothermal; Solar; Photocatalytic

1. Introduction

Photocatalysis is regarded as a cost-effective method for decomposing organic pollutants completely into harmless chemicals [1]. Bismuth-based oxides appear to be good candidates, because most of them respond strongly to visible light, owing to the interaction between Bi (6s) and O (2p) orbitals at the top of the valence band [2]. Bismuth tungstate (Bi_2WO_6, BW) is one of the simplest members of the Aurivillius oxide family and is a visible light-responsive photocatalytic material; however, the rapid recombination of photogenerated electron-hole pairs seriously limits its efficiency of energy

* Corresponding author.

conversion [3,4]. Designing efficient BW-based photocatalysts to oxidize organics remains a challenge.

Heterogeneous photocatalytic reactions normally occur on the surface of a photocatalyst or co-photocatalyst, which provides active reduction or oxidation sites to promote the separation of photogenerated electrons and holes. The species and properties of a co-photocatalyst importantly affect photocatalytic efficiency. In recent years, heterostructural composites of pairs of semiconductors have been recognized as promising in the development of highly efficient photocatalytic materials. The different bandgap potentials in heterostructures can induce irreversible charge carrier separation and transfer at the interface, weakening the recombination process and promoting efficient electron-hole separation, increasing photocatalytic activity [5–7]. To improve the photocatalytic activity of BW, an appropriate photocatalyst can be incorporated into it to broaden the spectral range of its visible light photoresponse or to promote the separation of carriers, as in TiO_2/BW [8–12], Bi_2O_3/BW [5–7,13,14], Bi_2S_3/BW [15,16], $BiVO_4$/BW [1,17–19], Bi_2MoO_6/BW [20], $BiFeO_3$/BW [21] and so on.

Chaiwichian et al. [18] synthesized $BiVO_4$/BW heterojunction photocatalysts using the hydrothermal method and found that the photocatalytic activity was highest at a $BiVO_4$: BW molar ratio of 0.5:0.5. The enhanced photocatalytic activity of $BiVO_4$/BW photocatalysts is attributable the improved charge separation with different energy levels of $BiVO_4$ and BW. Xue et al. [19] prepared $BiVO_4$/BW composite by solvothermal synthesis and found that $BiVO_4$/BW composite with a 50% molar percentage of $BiVO_4$ exhibited excellent photocatalytic activity. Their experimental results revealed that a photoinduced interfacial charge transfer process for separating and transporting the photogenerated electron-hole pairs has a critical role in the enhanced photocatalytic performance of the $BiVO_4$/BW composites. Ju et al. [1] synthesized $BiVO_4$/BW composite by a hydrothermal process that was followed by calcination at 873 K and found that it exhibited greater photocatalytic activity than $BiVO_4$, BW and un-calcined $BiVO_4$/BW in the degradation of rhodamine B (RhB). $BiFeO_3$/BW composites were prepared by the coupling of precipitation with hydrothermal methods and showed higher activity at the 1:1 molar ratio of $BiFeO_3$/BW than $BiFeO_3$ and BW [21]. Li et al. [6] synthesized Bi_2O_3/BW composites (BBWs) using a microwave-assisted hydrothermal method. Gui et al. [5] generated BBWs using a two-step solvothermal process with BW as the substrate. Hao et al. [14] synthesized BBWs via a solution combustion method. Photocatalytic experiments reveal that BBWs exhibit greater photocatalytic activity than Bi_2O_3 and BW [5–7,13,14].

Various methods were used to prepare heterojunction materials; they include the hydrothermal process, the sonochemical method, the solvothermal process, the solid-state reaction method, co-precipitation, the sol-gel method, microwave synthesis and chemical deposition. The solvothermal method can yield photocatalysts with a smaller particle size and a larger surface area than obtained using the hydrothermal method [11]. This study is the first to use the single-step solvothermal process to prepare BBWs. The photocatalytic activity of BBWs was evaluated by the photodegradation of C.I. Reactive Red 2 (RR2). The objectives of this study are (i) to synthesize BBWs with various Bi_2O_3/BW molar ratios; (ii) to measure the physicochemical properties and photocatalytic activities of the prepared BBWs; (iii) to determine the effects of photocatalyst dosage, RR2 concentration and pH on RR2 photodegradation and (iv) to compare the stability and reusability of BW with that of BBWs.

2. Materials and methods

2.1. Materials

Bismuth nitrate ($Bi(NO_3)_3{\cdot}5H_2O$) and sodium tungstate ($Na_2WO_4{\cdot}2H_2O$) were used as precursors in the formation of Bi and W, respectively, to generate BW (Katayama, Japan). Bismuth nitrate was also used as a precursor in the formation of Bi_2O_3. Ethylene glycol (EG) was used as a solvent in the solvothermal process (Katayama, Japan). RR2 ($C_{19}H_{10}Cl_2N_6Na_2O_7S_2$) was purchased from Sigma Aldrich (USA). To detect the active species that formed in the BBWs system, superoxide radicals, holes and hydroxyl radicals were detected by adding K_2CrO_4 (Katayama, Japan), ethylenediaminetetraacetic acid disodium salt (EDTA-2Na) (Katayama, Japan) and isopropanol (IPA) (J.T. Baker, USA), respectively. The pH of the solution was adjusted by adding 0.1 M HNO_3 or NaOH during the reaction, both of which reagents were purchased from Merck (USA). All reagents were of analytical purity and used without further purification.

2.2. Synthesis of Bi_2O_3, BW and BBWs

BW was prepared under conditions that were identified as optimal by Wu et al. [22]. 1.319 g sodium tungstate and the desired amount of bismuth nitrate were added to 70 mL EG and the resulting solution was vigorously magnetically stirred. The mixtures were adjusted to pH 2 by adding 10 M NaOH and stirring for 1 h. The mixtures were sealed in a 100 mL Teflon-lined stainless steel autoclave and heated at 433 K under self-generated pressure for 12 h; they then were allowed to cool naturally to room temperature. The precipitates were collected by filtration and washed using 50 mL 95% ethanol and 100 mL D.I. water to remove any residual impurities. The samples were finally dried in air at 333 K for 24 h. Bi_2O_3/BW with five molar ratios (0.05, 0.1, 0.25, 0.5 and 1) were synthesized and denoted as 0.05 BB, 0.1 BB, 0.25 BB, 0.5 BB and 1 BB, respectively. When no sodium tungstate was added, the obtained powder was pure Bi_2O_3. BW was prepared using a bismuth/tungsten molar ratio of 2. The experimental conditions and procedures for synthesizing Bi_2O_3 and BW were the same as those for generating BBWs.

2.3. Characterization of photocatalysts

The crystal phases of the photocatalysts were identified by X-ray diffraction (XRD) using a Bruker D8 SSS-Advance diffractometer (Germany) with Cu-Kα radiation (λ = 1.5406 Å) in the 2θ range of 20°–80°. The UV-vis diffusion reflectance spectra of the samples were analyzed using a UV-vis spectrophotometer (JAS.CO-V670, Japan) and used to calculate the bandgap energy of each photocatalyst. The morphology of each sample was observed by

scanning electron microscopy (SEM, JEOL 6330 TF, Japan) and transmission electron microscopy (TEM, JEOL 3010, Japan). Energy dispersive X-ray spectroscopy (EDS, Bruker Quantax 400 EDS) and EDS element mapping images were used to analyze the elemental compositions of 0.5BB. The Brunauer-Emmett-Teller (BET) surface area was obtained by measuring the nitrogen adsorption-desorption isotherms using a Micromeritics ASAP 2020 (USA) at a bath temperature of 77 K. The surface charge of BBWs in aqueous solution was measured using a zeta potential analyzer (BIC 90 plus, USA), and used to calculate the pH of the zero point of charge (pH_{zpc}). The surface compositions and chemical states were identified using a PHI 5000 Versa Probe X-ray photoelectron spectroscope (XPS) (USA). All of the binding energies were obtained from the XPS spectra following calibration by setting C_{1s} to 284.6 eV. The concentrations of RR2 were evaluated by measuring the absorbance of solutions at a wavelength of 538 nm using a UV-vis spectrophotometer (Hitachi U5100, Japan).

2.4. Decolorization experiments

All experimental runs were conducted at 298 K. The concentration of RR2 was 20 mg/L in all experiments except those performed to determine the effects of the RR2 concentration; the photocatalyst dosage was 0.5 g/L in all experiments except those carried out to determine the effects of the 0.5 BB dose; and the solution pH was 3 in all experiments except those performed to determine the effects of pH. In experiments with scavengers added, the initial concentration of each scavenger equaled the molar concentration of 0.5 g/L 0.5 BB. Decolorization experiments were performed in a 3 L hollow cylindrical glass reactor. A 400 W Xe lamp (200 nm < wavelength < 700 nm, UniVex BT-580, Taiwan) was used to provide simulated solar radiation. The intensity of the light from the lamp was 30.3 mW/cm^2. When the lamp was turned on, the RR2 removal corresponded to photodegradation, and when the lamp was turned off, the RR2 removal corresponded to adsorption. The reaction medium was stirred continuously at 300 rpm and aerated with air to maintain the suspension. Ten milliliter aliquots were withdrawn from the photoreactor at predetermined intervals. Suspended photocatalyst particles were separated by filtration through a 0.22 μm filter (Millipore, USA). Some experiments were conducted in triplicate and mean values are reported.

To identify the contribution of photodegradation and adsorption reactions to RR2 removal, the used Bi_2O_3 and 0.5 BB particles were collected for use in desorption experiments. 0.3 g used Bi_2O_3 or 0.5 BB was added to 300 mL NaOH solution at pH 12 to remove the RR2 that was adsorped onto the surface of the used Bi_2O_3 and 0.5 BB. To investigate the stability and reusability of BW and 0.5 BB, three cycles of photodegradation on RR2 were performed. After each cycle of photodegradation, the photocatalysts were separated from the solution by filtration and reused in the following run.

3. Results and discussion

3.1. Physical characterization of photocatalysts

Fig. 1 displays the XRD patterns of Bi_2O_3, BW and BBWs. The crystal structures of the BBWs with different Bi_2O_3 contents yielded similar diffraction peaks. The peaks at 28.3°, 32.8°, 47.0°, 55.8°, 76.1°, and 78.6° correspond to the (1 1 3), (2 0 0), (0 2 6), (3 1 3), (3 3 3), and (2 4 0) reflections of the crystal phases of BW (JCPDS No.73-1126), respectively. BW and BBWs exhibit good crystallinity; their distinct diffraction peaks corresponded to the orthorhombic BW phase and the peaks at 27.9°, 32.7°, 46.9° and 55.7° corresponded to the tetragonal Bi_2O_3 phase (JCPDS no.27-0050). The diffraction peaks of BBWs were similar to those of BW, revealing that the introduction of Bi_2O_3 did not alter the BW crystal structure. Notably, no diffraction peaks from Bi_2O_3 can be observed in the XRD patterns of BBWs, perhaps because of the close diffraction peaks of Bi_2O_3 and BW and the high dispersion of Bi_2O_3 particles in the BBWs. No significant shifts in the principal diffraction peaks were observed, indicating that the Bi_2O_3 was present as a separate phase rather than being incorporated into the BW lattice [5].

The morphologies of BW, Bi_2O_3 and 0.5 BB were studied using SEM (Fig. 2) and TEM (Fig. 3). SEM images revealed irregular nanoplate-like morphologies. These nanoplates crossed each other and aggregated (Fig. 2). The BW particles have diameters of about 10–30 nm and were ellipsoidal (Fig. 3(a)); the Bi_2O_3 particles have diameters of approximately 30–50 nm and were spherical (Fig. 3(b)). TEM images display many nanoparticles, which are anchored on the surface of the BW nanosheet and the smaller nanosheet should be BW (Fig. 3(c)). To confirm the composition of 0.5 BB, the 0.5 BB sample was characterized by TEM-EDS. The EDS results indicated that 0.5 BB contained only Bi, O and W elements and the Bi/W atomic ratio that was calculated from the EDS spectrum was approximately 74/26, which is close to the ideal value (Bi/W = 75/25) for the experimental design, revealing that Bi_2O_3 and BW were solvothermally synthesized with a similar rate.

Fig. 4 shows the UV-vis diffuse reflectance spectra of Bi_2O_3, BW and BBWs. According to the equation $E_g = 1240/\lambda$, where E_g denotes the bandgap energy and λ is the bandgap wavelength, λ is determined by the wavelength that corresponds to the intersection of the vertical and horizontal parts of the spectrum [9]. The absorption edges of the BBWs did

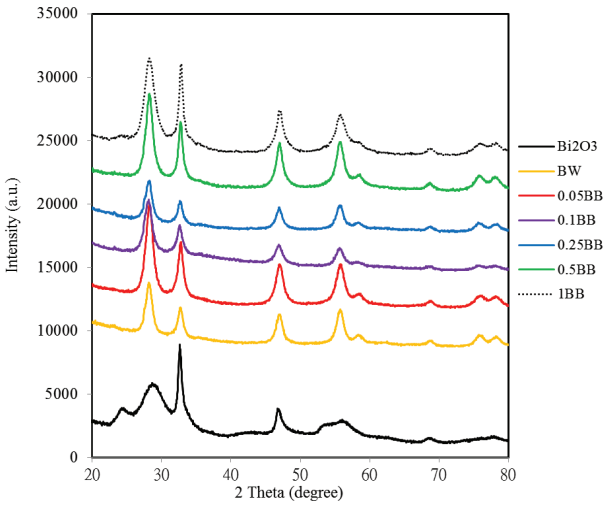

Fig. 1. XRD patterns of Bi_2O_3, BW and BBWs.

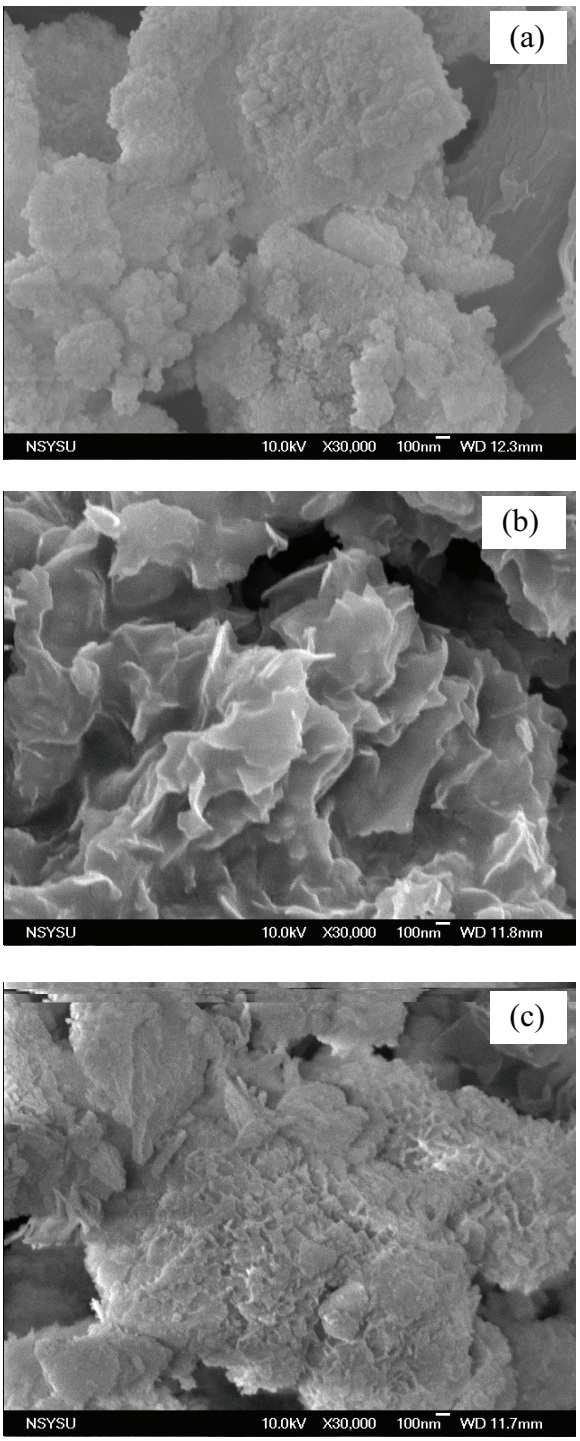

Fig. 2. SEM image of photocatalyst (a) BW (b) Bi_2O_3 (c) 0.5 BB.

not differ significantly from that of BW, which was approximately 495 nm (Fig. 4). Zhang et al. [17] also identified no obvious difference between the bandgap absorption edges of the $BiVO_4$ and $BiVO_4$/BW composites. The corresponding bandgaps of Bi_2O_3, BW, 0.05 BB, 0.1 BB, 0.25 BB, 0.5 BB and 1 BB are calculated to be 3.5, 2.9, 3.2, 3.2, 3.2, 3.2 and 3.3 eV, respectively (Table 1). The bandgap energies of the series of BBWs exceed that of BW and are less than that of Bi_2O_3.

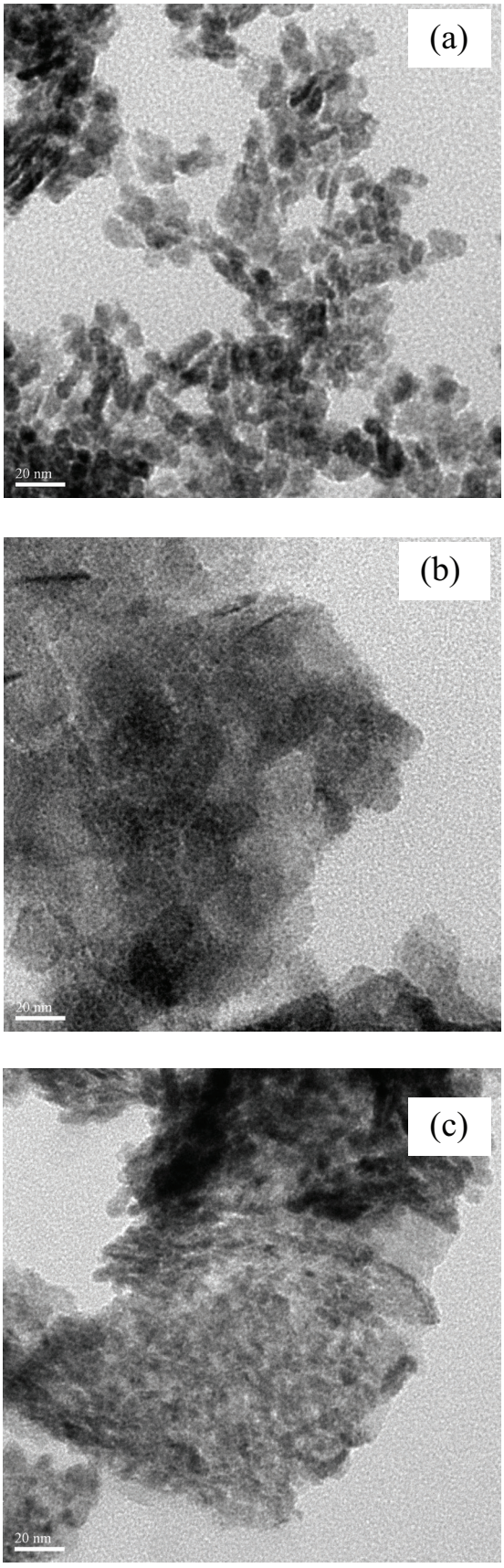

Fig. 3. TEM image of photocatalyst (a) BW (b) Bi_2O_3 (c) 0.5 BB.

XPS was conducted to determine the surface chemical composition and chemical states of 0.5BB. Figs. 5(a)–(c) display the XPS spectra of the Bi, W and O elements in the 0.5 BB. Two symmetric peaks of $Bi_{4f5/2}$ and $Bi_{4f7/2}$ were observed at 163.4 and 158.2 eV, respectively (Fig. 5(a)), indicating that all of the Bi in the 0.5 BB was in form of Bi^{3+} [23,24]. The XPS spectrum of W_{4f} exhibited two symmetric peaks of $W_{4f7/2}$ and $W_{4f5/2}$ at 34.2 and 36.4 eV respectively, suggesting that *W* was present in the state W^{6+} [5] (Fig. 5(b)). Owing to the presence of several types of nonequivalent lattice O atoms, the XPS spectrum in the O_{1s} region is complex and can be deconvoluted to four peaks at 530.8, 530.2, 529.0, and 531.6 eV (Fig. 5(c)), which are attributable to –OH [25], Bi–O [26] in Bi_2O_3 and Bi–O [6,27] and W–O [5] in BW, respectively. The results demonstrate the co-existence of Bi_2O_3 and BW consistent with the above XRD analysis. Based on the analysis of the O_{1s} region of the XPS spectrum of the BBWs, the –OH contents on the surfaces of BW, 0.05 BB, 0.1 BB, 0.25 BB, 0.5 BB and 1 BB were 19%, 10%, 11%, 7%, 10% and 9%, respectively. These XRD, SEM, TEM and XPS results clearly demonstrated the formation of heterojunctions between Bi_2O_3 and BW herein. The close contact between Bi_2O_3 and BW may facilitate the formation of BBWs heterojunctions, improving the carriers transfer rate and separation efficiency during photocatalysis [27].

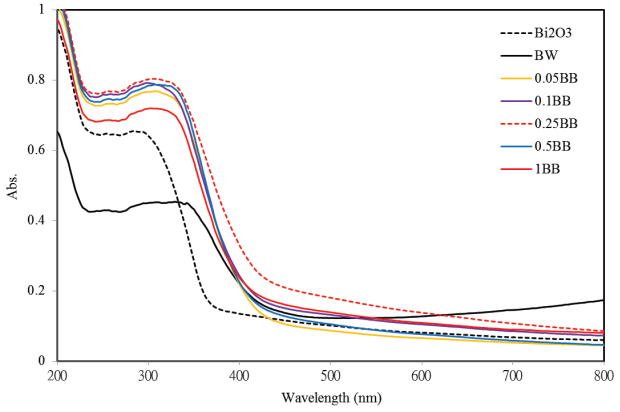

Fig. 4. UV-vis absorption spectra of SnO_2, BW and BBWs.

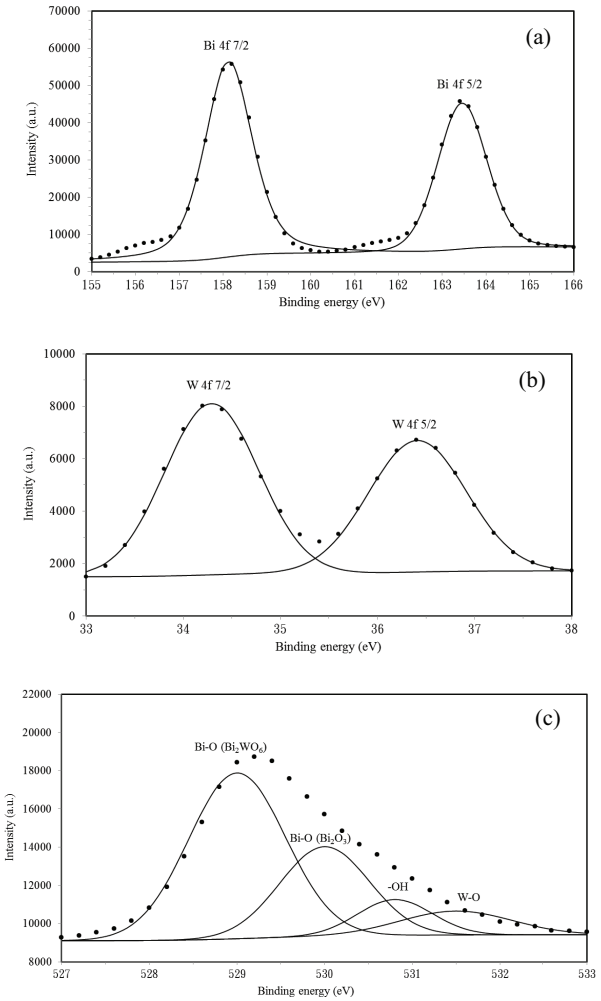

Fig. 5. XPS spectra of 0.5 BB (a) Bi_{4f} (b) W_{4f} (c) $O_{1s.}$

Table 1
Surface characteristics of prepared photocatalysts

Photocatalysts	BET surface area (m^2/g)	Bandgap (eV)	pH_{zpc}	k (min^{-1})	R^2
Bi_2O_3	45.4	3.5	4.4	0.1994	0.993
BW	100.3	2.9	2.2	0.0251	0.999
				(0.0155)[a]	(0.987)[a]
				(0.0152)[b]	(0.999)[b]
0.05 BB	91.1	3.2	3.2	0.0587	0.999
0.1 BB	82.5	3.2	3.4	0.0727	0.998
0.25 BB	72.5	3.1	3.5	0.0599	0.997
0.5 BB	71.0	3.2	3.3	0.1543	0.996
				(0.085)[a]	(0.999)[a]
				(0.0738)[b]	(0.999)[b]
1 BB	67.8	3.3	3.3	0.0995	0.994

[a]2nd run.
[b]3rd run.

3.2. Photocatalytic activity of Bi_2O_3, BW and BBWs

Figs. 6(a) and (b) present the removal of RR2 by adsorption and photodegradation, respectively. After 60 min of reaction, the percentages of RR2 adsorbed by Bi_2O_3, BW, 0.05 BB, 0.1 BB, 0.25 BB, 0.5 BB and 1 BB were 98%, 19%, 29%, 36%, 46%, 73% and 78%, respectively (Fig. 6(a)). The RR2 adsorption percentage increased with the Bi_2O_3 content of the BBWs. The pH_{zpc} of all BBWs exceeded that of BW (Table 1), indicating that coupling BW with Bi_2O_3 improved the adsorption of RR2 on the composites. After 60 min of reaction, the percentages of RR2 photodegraded by Bi_2O_3, BW, 0.05 BB, 0.1 BB, 0.25 BB, 0.5 BB and 1 BB were 100%, 81%, 98%, 97%, 97%, 98% and 100%, respectively (Fig. 6(b)). The photodegradation process followed pseudo-first-order kinetics, $\ln(C/C_0) = -k_t$, where C_0 is the initial concentration of RR2; C is the concentration of RR2 after it was irradiated by simulated solar light for a period of t; k is the photodegradation rate constant and t is the irradiation time [11,21,22]. The k values followed the order Bi_2O_3 > 0.5 BB > 1 BB > 0.1 BB > 0.25 BB > 0.05 BB > BW (Table 1). The percentages of RR2 adsorbed and photodegraded by Bi_2O_3 were almost equal. The photocatalytic activities of Bi_2O_3 and 0.5 BB were further clarified by performing desorption experiments.

The introduction of too little or too much Bi_2O_3 into BW did not contribute to the efficient separation of charge carriers, resulting in unsatisfactory activity. When the Bi_2O_3 loading is low, the separation efficiency of photogenerated electron-hole pairs is too low and the photocatalytic activity of the composite does not reach its maximum. Excess covering of BW with Bi_2O_3 would reduce the photocatalytic activity of BBWs because the interface of BBWs might act as the recombination centers for photogenerated carriers. Furthermore, excess cover of BW with Bi_2O_3 would reduce the absorption of light by BW. Apparently, 0.5 BB has the highest photocatalytic activity, which is approximately 6.1 times higher than that of BW.

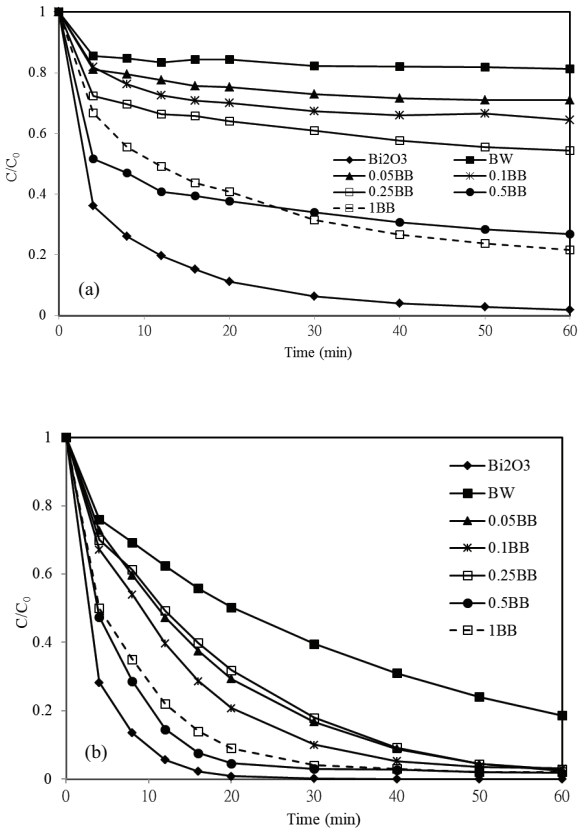

Fig. 6. Comparisons of RR2 removal by Bi_2O_3, BW and BBWs (a) adsorption (b) photodegradation ([RR2] = 20 mg/L, pH = 3, [photocatalyst] = 0.5 g/L).

The photocatalytic behavior of particles is well known to be closely related to their size and surface area. The surface areas of solvothermally synthesized BW and BBWs were higher than those of BW and BBWs that were prepared by mechanochemical activation [29]. A larger surface area is normally associated with smaller particles and a higher adsorption capacity, resulting in greater photocatalytic activity. The surface area of BW exceeds that of BBWs, whereas the photocatalytic performance of BW is weaker than that of BBWs (Table 1). The effect of the specific surface area of BBWs on its photocatalytic activity is negligible, as for a $BiFeO_3$/BW composite, possibly because the coexistence of $BiFeO_3$ and BW causes the separation of electron and whole pairs, enhancing photocatalytic activity [21].

Notably, the efficiencies of adsorption (98%) and photodegradation (100%) of RR2 by Bi_2O_3 were approximately equal. Upon the addition of a photocatalyst to the photocatalysis system, adsorption and photodegradation reactions proceeded simultaneously under light irradiation; however, without light irradiation, only adsorption occurred. Hence, the contributions of adsorption and photodegradation to the decolorization of RR2 needed to be clarified. The used Bi_2O_3 and 0.5BB after the adsorption and photodegradation experiments were collected for use in desorption experiments. Figs. 7(a) and (b) plot the results of desorption from used Bi_2O_3 and 0.5BB, respectively. The theoretical mass of RR2 desorption from the used Bi_2O_3 and 0.5BB after adsorption were 19.6 and 14.6 mg, respectively. The masses of RR2 desorbed from the used Bi_2O_3 after adsorption and photodegradation reactions were 15.8 and 1.7 mg, respectively, corresponding to 81% and 9% of the theoretical RR2 desorption, respectively (Fig. 7(a)). The obtained masses of RR2 desorption from the used 0.5 BB after adsorption and photodegradation reactions were 11.3 and 0.2 mg, respectively, corresponding to 77% and 1% of the theoretical RR2 desorption, respectively (Fig. 7(b)). The desorption results revealed that the adsorped RR2 on the surfaces of Bi_2O_3 and 0.5BB could be further removed by photodegradation; moreover, the photocatalytic efficiency of 0.5 BB greatly exceeded that of Bi_2O_3.

Figs. 8(a), (b) and (c) plot the effects of 0.5 BB dosage, RR2 concentration and pH on the RR2 photodegradation, respectively. The photodegradation efficiency of RR2 after 20 min of reaction increased from 82% to 99% as the 0.5 BB dose increased from 0.25 to 1 g/L (Fig. 8(a)). This phenomenon can be explained by the fact that the number of active photogenerated species increased with the photocatalyst dosage. The photodegradation efficiency of RR2 after 20 min of reaction fell from 98% to 63% as the initial RR2 concentration increased from 10 to 40 mg/L (Fig. 8(b)). The degradation efficiency declined as the initial RR2 concentration increased, perhaps because a significant fraction of light is harvested

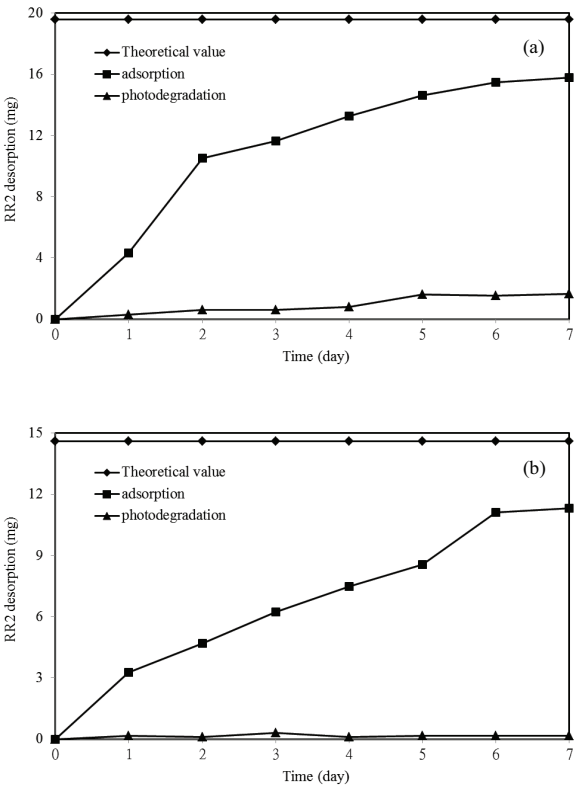

Fig. 7. Desorption experiments of used Bi_2O_3 and 0.5 BB (a) Bi_2O_3 (b) 0.5 BB.

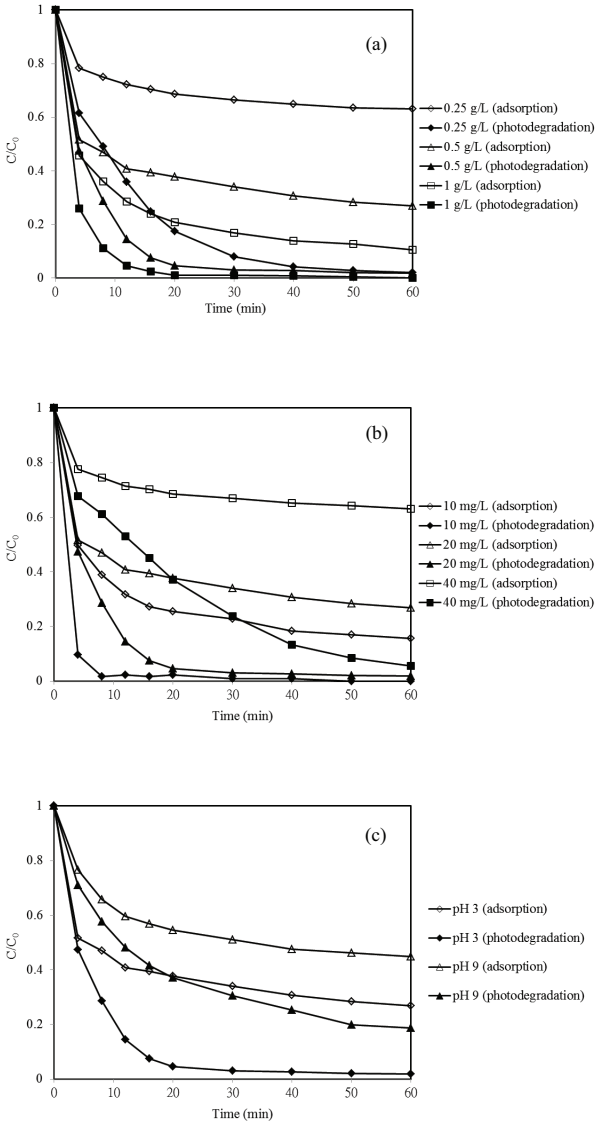

Fig. 8. Effects of 0.5 BB dose, RR2 concentration and pH on RR2 removal by 0.5 BB (a) 0.5 BB dose (b) RR2 concentration (c) pH.

by RR2 rather than 0.5BB in the presence of a high initial concentration of RR2. Another possible reason is that the products of the photocatalytic reaction may occupy some of the reactive sites on 0.5BB, inhibiting RR2 degradation [30]. The photodegradation efficiency of RR2 after 20 min reaction declined from 95% to 63% as the initial pH increased from 3 to 9 (Fig. 8(c)). The pH of the solution significantly influenced the surface charge of the photocatalyst, the electrostatic interaction between the photocatalyst surface and the RR2 molecules, and the number of charged radicals. The efficiency of adsorption of RR2 molecules onto the surface of 0.5 BB improved as the pH value decreased (Fig. 8(c)). When the pH value was relatively low, the surface of the BBWs tended to be positively charged, resulting in a relatively high adsorption of RR2. The higher adsorption of organic contaminants on the surface of photocatalysts leads to greater photocatalytic degradation; accordingly, powerful photocatalytic activity was observed at low pH values (pH 3).

To elucidate the active species of photodegradation, trapping experiments were performed using three sacrificial agents in the photocatalysis process. Cr(VI) was used as the photogenerated electron scavenger to determine whether superoxide radicals were present. Cr(VI) [31], EDTA-2Na [5,32] and IPA [5,32] were utilized as superoxide radicals, holes and hydroxyl radical scavengers, respectively. Fig. 9 plots the photodegradation of RR2 by 0.5 BB in the presence of different scavengers. The *k* values of 0.5 BB, IPA/0.5 BB, EDTA-2Na/0.5 BB and Cr(VI)/0.5 BB systems were 0.154, 0.153, 0.003 and 0.065 min^{-1}, respectively. IPA only weakly inhibited the photodegradation of RR2. Hence, holes and superoxide radicals were inferred to be the dominant active species in this photocatalytic system, and hydroxyl radicals played a minor role in the photocatalytic reaction. The enhanced photocatalytic activity of BBWs is attributed to the effective separation of electron-hole pairs between Bi_2O_3 and BW [6]. The photogenerated holes have been demonstrated to play a major role in the degradation of organic compounds over BBWs [5]. Ju et al. [1] suggested that the holes and hydroxyl radicals play key roles in the $BiVO_4$/BW system for RhB degradation. The photogenerated holes and superoxide radicals play critical roles in the photocatalytic process in an Ag_3VO_4/BW system [30] and Bi_2S_3/BW system [16], which were similar to the system in this study. Dong et al. [33] suggested that photogenerated holes are the dominant oxidative species in the degradation of RhB in reduced graphene oxide/BW composites, in which the hydroxyl and superoxide radicals have a minor role. Cheng et al. [34] found that superoxide radicals,

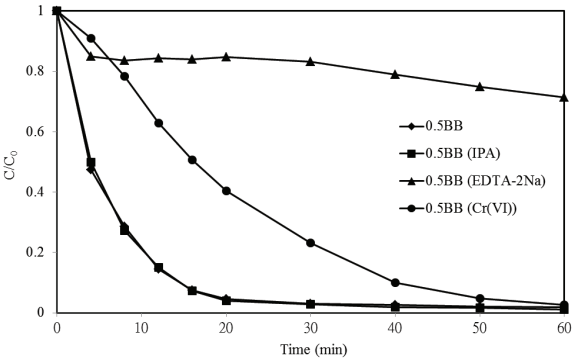

Fig. 9. Photodegradation of RR2 by 0.5 BB in the presence of different scavengers ([RR2] = 20 mg/L, pH = 3, [0.5 BB] = 0.5 g/L).

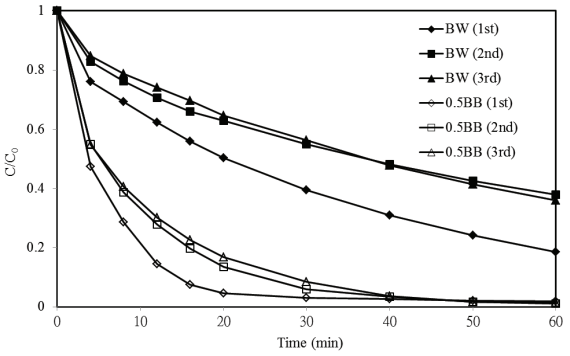

Fig. 10. Profiles of cyclic photocatalysis for RR2 in BW and 0.5 BB systems ([RR2] = 20 mg/L, pH = 3, [photocatalyst] = 0.5 g/L).

rather than holes and hydroxyl radicals, are the major species during photocatalysis. The involvement of active radicals in the BW suspension is disputed; the roles of holes and superoxide radicals in the degradation pathways have been widely reported, whereas the participation of hydroxyl radicals is seldom discussed [35]. The hydroxyl and superoxide radicals play important roles in the photocatalytic processes of $CaSn(OH)_6$ [36], AgBr-Ag-BW [37] and In_2O_3/TiO_2 [38] systems. Superoxide radicals are the major active reagent in TiO_2/Eosin Y/Rhodamine B [39] and TiO_2 [40] systems. This study suggested that the active species of photodegradation varied with the photocatalyst.

The estimation of reusability and stability is of utmost practical importance. Recycling runs of RR2 degradation over BW and 0.5 BB were performed to evaluate the photocatalytic stability of these systems (Fig. 10). Over three cycles, the proportion of RR2 that was photodegraded by BW in 60 min of reaction fell from 81% to 64%, and that photodegraded by 0.5 BB fell from 98% to 97% (Fig. 10). The k values of BW in runs 1, 2 and 3 were 0.0251, 0.0155 and 0.0152 min^{-1}, respectively, and those of 0.5 BB in runs 1, 2 and 3 were 0.1543, 0.085 and 0.0738 min^{-1}, respectively (Table 1). In each run, the rate of RR2 photodegradation by 0.5BB exceeded that by BW. 0.5 BB does not exhibit significant loss of activity after three cycles of photodegradation of RR2, revealing that 0.5 BB has good stability and reusability.

3.3. Possible photocatalytic mechanism

The photocatalytic activity of BW was enhanced by coupling it with semiconductors that improved the charge carrier separation; carrier transfer depended on the positions of the conduction and valence bands (CB and VB) in the heterostructural composite [35]. To provide insight into the mechanism of the improvement of the photocatalytic activity of the BBWs, the positions of the CB and VB were calculated using the following empirical equation (Eqs. (1) and (2)). The potentials of the CB and VB edges of Bi_2O_3 and BW were obtained using the equation that relates the Mulliken electronegativity and the bandgap of a photocatalyst [6,41,42],

$$E_{CB} = X - E_e - 0.5\,E_g \quad (1)$$

$$E_{VB} = E_{CB} + E_g \quad (2)$$

where E_{CB}, E_{VB} and E_g are the bottom energy of CB and VB relative to the NHE level and the bandgap of the photocatalyst, respectively; X is the geometric mean of the Mulliken electronegativities of the constituent atoms in the photocatalyst, and E_e is the energy of free electrons on the hydrogen scale (4.5 eV) [41]. The X values for BW and Bi_2O_3 are 6.20 and 5.92 [42], respectively, and the bandgap energies of BW and Bi_2O_3 are 2.9 and 3.5 eV, respectively (Table 1). The E_{CB} values of BW and Bi_2O_3 are determined to be 0.25 and –0.33 eV relative to the NHE level, respectively. Correspondingly, the E_{VB} values of BW and Bi_2O_3 are obtained as 3.15 and 3.83 eV, respectively. In the BBWs, only BW was excited by simulated solar light irradiation. Under simulated solar irradiation, electrons in the VB of BW were excited to the CB of BW, leaving the same amount of holes in the VB of BW. Then, electrons in the CB of BW were injected into the VB of Bi_2O_3 because the CB of BW is more negative than the VB of Bi_2O_3. This transference can effectively suppress the recombination of electron-hole pairs, enhancing the photocatalytic activity of BBWs over that of pure BW and Bi_2O_3. Meanwhile, numerous photogenerated holes that are accumulated in the VB of BW can directly decompose RR2. The resulting separation of photogenerated electrons and holes may facilitate the transfer of charge carriers and retard the recombination of electron-hole pairs, improving photocatalytic performance [6]. Bing et al. [28] indicated that photogenerated electrons in the CB of BW are transferred to the VB of Bi_2O_3, effectively preventing the recombination of electrons and holes in Bi_2O_3 and BW. The findings of this study were similar to those of Bing et al. [28]. However, Hao et al. [14] suggested that the enhanced activity is attributable to the transfer of electrons from Bi_2O_3 to BW. The differences can be attributed to the different methods for synthesizing BBWs that were used in this study and that of Hao et al. [14].

4. Conclusions

In this study, BBWs with high photocatalytic activity were synthesized. The XRD, SEM, TEM and XPS results strongly revealed the formation of heterojunctions between Bi_2O_3 and BW, and coupling Bi_2O_3 on BW improved the adsorption of

RR2 on BBWs. The RR2 photodegradation rate constants followed the order Bi_2O_3 > 0.5 BB > 1 BB > 0.1 BB > 0.25 BB > 0.05 BB > BW. 0.5 BB exhibited a high separation efficiency of the photogenerated electron-hole pairs, effectively suppressing the recombination of electrons and holes, extending the lifetime of the charge carriers and enhancing the efficiency of photodegradation of RR2.

Acknowledgement

The authors would like to thank the Ministry of Science and Technology and National Kaohsiung University of Science and Technology, for financially supporting this research under Contract No. MOST 107-2221-E-992-001-MY2 and 107M01-1, respectively.

References

[1] P. Ju, P. Wang, B. Li, H. Fan, S. Ai, D. Zhang, Y. Wang, A novel calcined Bi_2WO_6/$BiVO_4$ heterojunction photocatalyst with highly enhanced photocatalytic activity, Chem. Eng. J., 236 (2014) 430–437.

[2] T. Saison, N. Chemin, C. Chaneac, O. Durupthy, V. Ruaux, L. Mariey, F. Mauge, P. Beaunier, J.P. Jolivet, Bi_2O_3, $BiVO_4$, and Bi_2WO_6: impact of surface properties on photocatalytic activity under visible light, J. Phys. Chem. C., 115 (2011) 5657–5666.

[3] D. Ma, S. Huang, W. Chen, S. Hu, F. Shi, K. Fan, Self-assembled three-dimensional hierarchical umbilicate Bi_2WO_6 microspheres from nanoplates: controlled synthesis, photocatalytic activities, and wettability, J. Phys. Chem. C., 113 (2009) 4369–4374.

[4] M.S. Gui, W.D. Zhang, Y.Q. Chang, Y.X. Yu, One-step hydrothermal preparation strategy for nanostructured WO_3/Bi_2WO_6 heterojunction with high visible light photocatalytic activity, Chem. Eng. J., 197 (2012) 283–288.

[5] M.S. Gui, W.D. Zhang, Q.X. Su, C.H Chen, Preparation and visible light photocatalytic activity of Bi_2O_3/Bi_2WO_6 heterojunction photocatalysts, J. Solid. State. Chem., 184 (2011) 1977–1982.

[6] Z.Q. Li, X.T. Chen, Z.L. Xue, Microwave-assisted synthesis and photocatalytic properties of flower-like Bi_2WO_6 and Bi_2O_3–Bi_2WO_6 composite, J. Colloid. Interface. Sci., 394 (2013) 69–77.

[7] W. He, Y. Sun, G. Jiang, H. Huang, X. Zhang, F. Dong, Activation of amorphous Bi_2WO_6 with synchronous Bi metal and Bi_2O_3 coupling: photocatalysis mechanism and reaction pathway, Appl. Catal., B., 232 (2018) 340–347.

[8] Y. Liu, H. Tang, H. Lv, P. Zhang, Z. Ding, S. Li, J. Guang, Facile hydrothermal synthesis of TiO_2/Bi_2WO_6 hollow microsphere with enhanced visible-light photoactivity, Powder. Technol., 283 (2015) 246–253.

[9] Z. Du, C. Cheng, L. Tan, J. Lan, S. Jiang, L. Zhao, R. Guo, Enhanced photocatalytic activity of Bi_2WO_6/TiO_2 composite coated polyester fabric under visible light irradiation, Appl. Surf. Sci., 435 (2018) 626–634.

[10] Q. Guo, Y. Huang, H. Xu, D. Luo, F. Huang, L. Gu, Y. Wei, H. Zhao, L. Fan, J. Wu, The effects of solvent on photocatalytic properties of Bi_2WO_6/TiO_2 heterojunction under visible light irradiation, Solid. State. Sci., 78 (2018) 95–106.

[11] X. Song, H. Wang, Y. Li, S. Ye, D.D. Dionysiou, Solvothermal synthesis of P25/Bi_2WO_6 nanocomposite photocatalyst and photocatalytic degradation of ethylene under visible light, Appl. Surf. Sci., 439 (2018) 815–822.

[12] L. Yuan, K.Q. Lu, F. Zhang, X. Fu, Y.J. Xu, Unveiling the interplay between light-driven CO_2 photocatalytic reduction and carbonaceous residues decomposition: a case study of Bi_2WO_6-TiO_2 binanosheets, Appl. Catal. B., 237 (2018) 424–431.

[13] M.S. Gui, W.D. Zhang, A facile preparation strategy for hollow-structured Bi_2O_3/Bi_2WO_6 heterojunction with high visible light photocatalytic activity, J. Phys. Chem. Solids., 73 (2012) 1342–1349.

[14] Y.J. Hao, F.T. Li, F. Chen, M.J. Chai, R.H. Liu, X.J. Wang, In situ one-step combustion synthesis of Bi_2O_3/Bi_2WO_6 heterojunctions with notable visible light photocatalytic activities, Mater. Lett., 124 (2014) 1–3.

[15] Q. Zhang, Z. Dai, G. Cheng, Y. Liu, R. Chen, In-situ room-temperature synthesis of amorphous/crystalline contact Bi_2S_3/Bi_2WO_6 heterostructures for improved photocatalytic ability, Ceram. Int., 43 (2017) 11296–11304.

[16] S. Adhikari, D.H. Kim, Synthesis of Bi_2S_3/Bi_2WO_6 hierarchical microstructures for enhanced visible light driven photocatalytic degradation and photoelectrochemical sensing of ofloxacin, Chem. Eng. J., 354 (2018) 692–705.

[17] X. Zhang, Y. Gong, X. Dong, X. Zhang, C. Ma, F. Shi, Fabrication and efficient visible light-induced photocatalytic activity of Bi_2WO_6/$BiVO_4$ heterojunction, Mater. Chem. Phys., 136 (2012) 472–476.

[18] S. Chaiwichian, B. Inceesungvorn, K. Wetchakun, S. Phanichphant, W. Kangwansupamonkon, N. Wetchakun, Highly efficient visible-light-induced photocatalytic activity of Bi_2WO_6/$BiVO_4$ heterojunction photocatalysts, Mater. Res. Bull., 54 (2014) 28–33.

[19] S. Xue, Z. Wei, X. Hou, W. Xie, S. Li, X. Shang, D. He, Enhanced visible-light photocatalytic activities and mechanism insight of $BiVO_4$/Bi_2WO_6 composites with virus-like structures, Appl. Surf. Sci., 355 (2015) 1107–1115.

[20] F.J. Zhang, S.F. Zhu, F.Z. Xie, J. Zhang, Z.D. Meng, Plate-on-plate structured Bi_2MoO_6/Bi_2WO_6 heterojunction with high-efficiently gradient charge transfer for decolorization of MB, Sep. Purif. Technol., 113 (2013) 1–8.

[21] S. Chaiwichian, K. Wetchakun, W. Kangwansupamonkon, N. Wetchakun, Novel visible-light-driven $BiFeO_3$-Bi_2WO_6 nanocomposites toward degradation of dyes, J. Photochem. Photobiol. A., 349 (2017) 183–192.

[22] C.H. Wu, C.Y. Kuo, J.T. Wu, M.J. Hsu, T.J. Jhang, Photodegradation of C.I. Reactive Red 2 in the Bi_2WO_6 system: determination of surface characteristics and photocatalytic activities of Bi_2WO_6, React. Kinet. Mech. Catal., 117 (2016) 391–404.

[23] Y. Lu, K. Zhao, Y. Zhao, S. Zhu, X. Yuan, M. Huo, Y. Zhang, Y. Qiu, Bi_2WO_6/TiO_2/Pt nanojunction system: a UV-vis light responsive photocatalyst with high photocatalytic performance, Colloids. Surf., 481 (2015) 252–260.

[24] C. Yu, W. Zhou, L. Zhu, G. Li, K. Yang, R. Jin, Integrating plasmonic Au nanorods with dendritic like α-Bi_2O_3/$Bi_2O_2CO_3$ heterostructures for superior visible-light-driven photocatalysis, Appl. Catal., B., 184 (2016) 1–11.

[25] L. Yue, S. Wang, G. Shan, W. Wu, L. Qiang, L. Zhu, Novel MWNTs-Bi_2WO_6 composites with enhanced simulated solar photoactivity toward adsorbed and free tetracycline in water, Appl. Catal., B., 176–177 (2015) 11–19.

[26] T. Li, S. Luo, Hydrothermal synthesis of Ag_2O/Bi_2O_3 microspheres for efficient photocatalytic degradation of Rhodamine B under visible light irradiation, Ceram. Int., 41 (2015) 13135–13146.

[27] R. Hu, X. Xiao, S.Tu, X. Zuo, J. Nan, Synthesis of flower-like heterostructured β-Bi_2O_3/$Bi_2O_2CO_3$ microspheres using $Bi_2O_2CO_3$ self-sacrifice precursor and its visible-light-induced photocatalytic degradation of o-phenylphenol, Appl. Catal., B., 163 (2015) 510–519.

[28] X. Bing, J. Li, J. Liu, X. Cui, F. Ji, Biomimetic synthesis of Bi_2O_3/Bi_2WO_6/MgAl-CLDH hybrids from lotus pollen and their enhanced adsorption and photocatalysis performance, J. Photochem. Photobiol., A., 364 (2018) 449–460.

[29] P. Zhang, X. Teng, X. Feng, S. Ding, G. Zhang, Preparation of Bi_2WO_6 photocatalyst by high-energy ball milled Bi_2O_3-WO_3 mixture, Ceram. Int., 42 (2016) 16749–16757.

[30] S. Li, S. Hu, W. Jiang, Y. Liu, J. Liu, Z. Wang, Facile synthesis of flower-like Ag_3VO_4/Bi_2WO_6 heterojunction with enhanced visible-light photocatalytic activity, J. Colloid. Interface. Sci., 501 (2017) 156–163.

[31] Y. Chen, S. Yang, K. Wang, L. Lou, Role of primary active species and TiO_2 surface characteristic in UV-illuminated photodegradation of Acid Orange 7, J. Photochem. Photobiol., A., 172 (2005) 47–54.

[32] H. Huang, K. Liu, K. Chen, Y. Zhang, Y. Zhang, S. Wang, Ce and F comodification on the crystal structure and enhanced photocatalytic activity of Bi_2WO_6 photocatalyst under visible light irradiation, J. Phys. Chem. C., 118 (2014) 14379–14387.
[33] S. Dong, X. Ding, T. Guo, X. Yue, X. Han, J. Sun, Self-assembled hollow sphere shaped Bi_2WO_6/RGO composites for efficient sunlight-driven photocatalytic degradation of organic pollutants, Chem. Eng. J., 316 (2017) 778–789.
[34] J. Cheng, Y. Shen, K. Chen, X. Wang, Y. Guo, X. Zhou, R. Bai, Flower-like Bi_2WO_6/ZnO composite with excellent photocatalytic capability under visible light irradiation, Chin. J. Catal., 39 (2018) 810–820.
[35] S.G. Kumar, K.S.R.K. Rao, Tungsten-based nanomaterials (WO_3 & Bi_2WO_6): modifications related to charge carrier transfer mechanisms and photocatalytic applications, Appl. Surf. Sci., 355 (2015) 939–958.
[36] S.G. Meng, D.Z. Li, M. Sun, W.J. Li, J.X. Wang, J. Chen, X.Z. Fu, G.C. Xiao, Sonochemical synthesis, characterization and photocatalytic properties of a novel cube-shaped $CaSn(OH)_6$, Catal. Commun., 12 (2011) 972–975.
[37] L.S. Zhang, K.H. Wong, H.Y. Yip, C. Hu, J.C. Yu, C.Y. Chan, P.K. Wong, Effective photocatalytic disinfection of E. coli K-12 using AgBr-Ag-Bi_2WO_6 nanojunction system irradiated by visible light: the role of diffusing hydroxyl radicals, Environ. Sci. Technol., 44 (2010) 1392–1398.
[38] J. Zhong, J. Li, J. Zeng, X. He, S. Huang, W. Jiang, M. Li, Enhanced photocatalytic activity of In_2O_3-decorated TiO_2, Appl. Phys. A., 115 (2014) 1231–1238.
[39] M.C. Yin, Z.S. Li, J.H. Kou, Z.G. Zou, Mechanism investigation of visible light-Induced degradation in a heterogeneous TiO_2/Eosin Y/Rhodamine B system, Environ. Sci. Technol., 43 (2009) 8361–8366.
[40] X. Zheng, Q. Yang, S. Huang, J. Zhong, J. Li, R. Yang, Y. Zhang, Enhanced separation efficiency of photo-induced charge pairs and sunlight-driven photocatalytic performance of TiO_2 prepared with the assistance of NH_4Cl, J. Sol-Gel. Sci. Technol., 83 (2017) 174–180.
[41] T.P. Cao, Y.J. Li, C.H. Wang, Z.Y. Zhang, M.Y. Zhang, C.L. Shao, Y.C. Liu, $Bi_4Ti_3O_{12}$ nanosheets/TiO_2 submicron fibers heterostructures: in situ fabrication and high visible light photocatalytic activity, J. Mater. Chem., 21 (2011) 6922–6927.
[42] X. Meng, Z. Zhang, Bismuth-based photocatalytic semiconductors: introduction, challenges and possible approaches, J. Mol. Catal. A: Chem., 423 (2016) 533–549.